JACS
JOURNAL OF THE AMERICAN CHEMICAL SOCIETY
Article
pubs.acs.org/JACS

Elastic Frustration Causing Two-Step and Multistep Transitions in Spin-Crossover Solids: Emergence of Complex Antiferroelastic Structures

Miguel Paez-Espejo, Mouhamadou Sy, and Kamel Boukheddaden*

Groupe d'Etudes de la Matière Condensée, UMR 8635, Université Paris-Saclay, CNRS, 78035 Versailles, France

Supporting Information

ABSTRACT: Two-step and multistep spin transitions are frequently observed in switchable cooperative molecular solids. They present the advantage to open the way for three- or several-bit electronics. Despite extensive experimental studies, their theoretical description was to date only phenomenological, based on Ising models including competing ferro- and antiferro-magnetic interactions, even though it is recognized that the elastic interactions are at the heart of the spin transition phenomenon, due to the volume change between the low- and high-temperature phases. To remedy this shortcoming, we designed the first consistent elastic model, taking into account both volume change upon spin transition and elastic frustration. This ingredient was revealed to be powerful, since it was able to obtain all observed experimental configurations in a consistent way. Thus, according to the strength of the elastic frustration, the system may undergo first-order transition with hysteresis, gradual, hysteretic two-step or multistep transitions, and incomplete transitions. Furthermore, the analysis of the spatial organization of the HS and LS species in the plateau regions revealed the emergence of complex antiferro-elastic patterns going from simple antiferro-magnetic-like order to long-range spatial modulations of the high-spin fraction. These results enabled us to identify the elastic frustration as the fundamental mechanism at the origin of the very recent experimental observations showing the existence of organized spatial modulations of the high-spin fraction inside the plateau of two-step spin transitions.

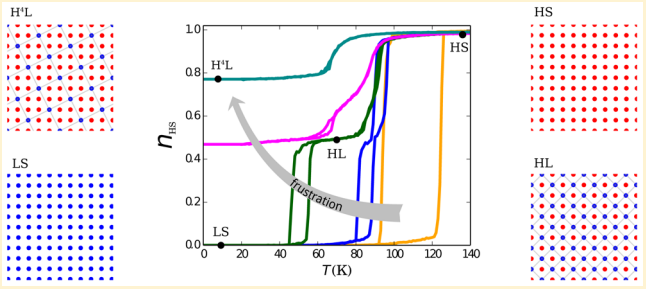

1. INTRODUCTION

Fe(II)-based spin-crossover (SC) materials,[1] converting between diamagnetic low-spin (LS, $e_g^0t_{2g}^6$) and paramagnetic high-spin (HS, $e_g^2t_{2g}^4$) states, are known to exhibit a rich variety of thermal behaviors, going from (i) gradual conversions to (ii) first-order transformations accompanied by hysteresis loops[2] as well as (iii) two-step or multistep phase transitions.[3−6] SC solids are known to have potential applications such as reversible high density memories, ultrafast switches (at the nanoscale), sensors of temperature and pressure, displays,[7−14] etc. From the theoretical viewpoint, elastic models[15−23] have been very efficient in the general description of SC materials. For example, the elastic models were able to find out the thermal hysteresis loops related to first-order SC phase transition as well as their non-linear relaxation at low-temperature from the photoinduced metastable states. The macroscopic nucleation, growth, and propagation of the front transformation, observed experimentally in several examples of spin-crossover single crystals, were also well described using electro-elastic and mechano-elastic models accounting for the unit cell volume change at the transition and for the long-range nature of the interactions in these systems. Despite this success, the two-step spin transitions observed experimentally in a tremendous number of systems remained a challenging problem, for which no consistent elastic description was furnished to date. Historically, the two-step spin transitions were described by Ising-like Hamiltonians[24−27] or atom phonon coupling models,[28] as well as by some recent hybrid models combining elastic and antiferro-magnetic Ising interactions,[29] leading to competing interactions. Although very instructive, these descriptions remain qualitative and do not capture the essential physical mechanism of the two-step spin transition. Thus, a consistent model should include only elastic interactions between SC units from which competing long-range ferro- and antiferro-elastic interactions should emerge as a result of the minimization of the internal strain. That is the objective assigned to the current work, in which we consider the elastic frustration at the origin of the existence of the two-step transitions. The crucial point here is to account for the existence of an elastic frustration when the system converts from HS to LS. From the structural point of view, the elastic frustration may arise from steric effects between ligands[30] which hinder some degree of freedom, or from the existence of strong covalent bonds in some direction around the metal center, which constrains the unit cell deformation. This concept opens a huge number of possibilities: the frustration can be included on nearest-neighboring (nn) atoms or next-nearest neighbors

Received: January 4, 2016
Published: February 9, 2016

DOI: 10.1021/jacs.6b00049
J. Am. Chem. Soc. 2016, 138, 3202−3210

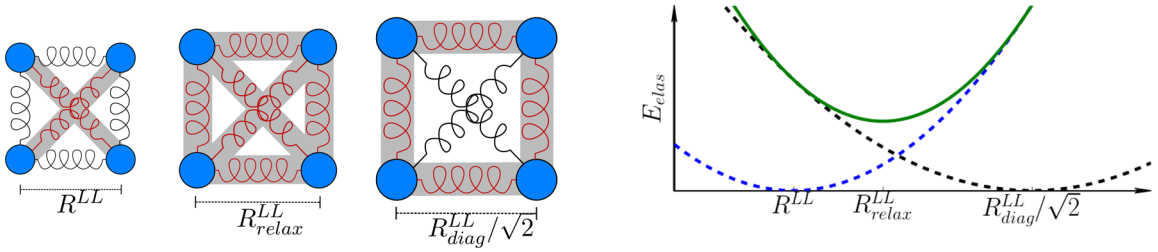

Figure 1. From left to right: LS unit cell configurations correspond to $x = R^{LL}$, R^{LL}_{relax} (relaxed mechanical state), and $R^{LL}_{d}/(2)^{1/2}$. Red springs are under tension and black ones are at equilibrium. Right panel: elastic energies $E_{elas}(x)$ associated with the previous three situations, easily identified by their x values at their minima. In the relaxed elastic configuration (green curve) nn and nnn bonds stay frustrated.

(nnn) depending on the lattice symmetry. In previous studies, performed on 2D systems with square symmetry, the interaction between the nnn (neighbors along the diagonal) has been considered with the aim to only keep the structure stable. Here, we give an active role to the nnn interaction along which the system experiences elastic frustration in the isotropic way.

2. ELECTRO-ELASTIC MODEL WITH ELASTIC FRUSTRATION

The electro-elastic model accounting for the volume change between the spin transition units is written as a set of fictitious spins, which mimic the two states of the SC molecules linked by springs. The total Hamiltonian, in 2D square symmetry, is given by

$$\mathcal{H} = \sum_i \left(\Delta - \frac{1}{2}k_B T \ln g\right)\sigma_i + \mathcal{H}_{elas} \tag{1}$$

where σ is the fictitious spin whose eigenvalues +1 and −1 are respectively associated with the LS and HS states of the molecule, Δ is the ligand field gap, g is the degeneracy ratio between the HS and LS states, which results in a temperature-dependent field,[31] T is the temperature, and k_B is the Boltzmann constant. The second term, $\mathcal{H}_{elas}$, in (eq 1) is the elastic contribution of the lattice, which is written as,

$$\mathcal{H}_{elas} = V_{nn}(|\vec{r}|) + V_{nnn}(|\vec{r}|) = \sum_{i,j}\frac{A}{2}(r_{ij} - R(\sigma_i, \sigma_j))^2 + \sum_{i,k}\frac{B}{2}(r_{ik} - R_d(\sigma_i, \sigma_k))^2 \tag{2}$$

Here, A and B are the elastic constants connecting nn and nnn atoms, respectively, and r_{ij} and r_{ik} are the respective nn and nnn instantaneous distances between sites. The indexes i and j (respectively, k) run over nn (respectively, nnn) sites. $R(\sigma_i, \sigma_j)$ is the equilibrium bond lengths between two nn nodes i and j, written so as to depend on their spin states: $R(+1,+1) = R^{HH}$, $R(-1,-1) = R^{LL}$, and $R(+1,-1) = R(-1,+1) = R^{HL} = (R^{LL} + R^{HH})/2$, where R^{HH}, R^{HL}, and R^{LL} are the respective equilibrium distances between HS-HS (HH), HS-LS (HL), and LS-LS (LL) sites. We denote by $\delta_R = R^{HH} - R^{LL}$, the lattice constant misfit between the HS and the LS lattices. The nnn equilibrium distance along the diagonals $R_d(\sigma_i, \sigma_k)$ depends on the spin states of the linked sites i and k, and is written so as to have a nonfrustrated bond-length in the HS state and induces an elastic frustration in HS-LS and LS-LS configurations. Let us denote by ξ (>0), the frustration rate along the diagonals. We assume a linear dependence of $R_d(\sigma_i, \sigma_k)$ with ξ, which will be written to have stress-free nnn equilibrium distances ($R_d(\sigma_i, \sigma_k) = R(\sigma_i, \sigma_k)(2)^{1/2}$) for $\xi = 0$ and $R_d(\sigma_i, \sigma_k) = R^{HH}(2)^{1/2}$ for $\xi = 1$. There is a unique ξ-dependence of $R_d(\sigma_i, \sigma_k)$ satisfying the previous perequisites (see demonstration in the Appendix I of the Supporting Information = SI). So, the equilibrium distances satisfying these prerequisites are

$$R(\sigma_i, \sigma_j) = R^{HL} + \frac{\delta_R}{4}(\sigma_i + \sigma_j)$$
$$R_d(\sigma_i, \sigma_k) = \sqrt{2}R(\sigma_i, \sigma_k) + (2 - (\sigma_i + \sigma_k))\sqrt{2}\frac{\delta_R}{4}\xi \tag{3}$$

As a result, the equilibrium distances (see eq 3) along the diagonals in the LL and HL configurations, respectively given by

$$R_d(-1,-1) = R^{LL}_d = \sqrt{2}R^{LL} + \sqrt{2}\delta_R\xi \quad \text{and}$$
$$R_d(+1,-1) = R^{HL}_d = \sqrt{2}R^{HL} + \sqrt{2}\frac{\delta_R}{2}\xi \tag{4}$$

are in both cases bigger than their respective usual equilibrium values for a nonfrustrated system, i.e., $(2)^{1/2}R^{LL}$ and $(2)^{1/2}R^{HL}$.

It is worth noticing that the frustration may also exist even for $\xi = 0$ in the rigid square lattice. Obviously, when the system is in the macroscopic HS or LS phases, the elastic energy is equal to zero, because all distances (between nn and nnn) are at equilibrium. In contrast, in the nonrelaxed antiferro-elastic (AF) configuration (HS-LS-HS-LS···), in which each HS (respectively, LS) site is surrounded by LS (respectively, HS) neighbors, for which nn (respectively, nnn) equilibrium distances are equal to R^{HL} (R^{HH} $(2)^{1/2}$ and R^{LL} $(2)^{1/2}$), a spontaneous stress is systematically generated (the minimum elastic energy is nonzero) in the unit cell. The equilibrium lattice constant, a, is determined so as to minimize the total energy of the rigid square structure, i.e., $V_{tot}(a) = 2N[V_{nn}(a) + V_{nnn}((2)^{1/2}a)]$ for a system of N atoms. Only with the condition of energy minimization $dV_{tot}(a)/da = 0$, does a spontaneous stress remain in the crystal: $\sigma_0 = -V'_{nn}(a) = (2)^{1/2}V'_{nnn}((2)^{1/2}a)$. The calculated equilibrium distance, a, in this case is $a = R^{HL}$, and the associated relaxed elastic energy is nonzero and is equal to $E^{AF,elas}_{relax} = 2B\delta_R{}^2$.

According to eq 3, for $\xi = 1$, the HS state has a minimum elastic energy equal to zero because equilibrium distance for nnn (respectively, nn) becomes R^{HH} $(2)^{1/2}$ (respectively, R^{HH}). In contrast, the HL and LS configurations have nnn (respectively, nn) equilibrium distances also equal to $R^{HH}(2)^{1/2}$ (respectively, R^{HL}) and $R^{HH}(2)^{1/2}$ (respectively, R^{LL}), respectively. Consequently, these two macroscopic states (AF and LS) remain always frustrated with a nonzero residual elastic energy, as soon as $\xi \neq 0$. The same situation holds for ξ

DOI: 10.1021/jacs.6b00049
J. Am. Chem. Soc. 2016, 138, 3202−3210

$\neq 1$, where the LS and the AF phases stay frustrated even at their minimal elastic energies, owing to the incompatibility between the nn and nnn equilibrium distances.

To well document and predict these elastic features, we study the elastic behavior of a rigid square of SC atoms whose total elastic energy (see Appendix II in the SI) is written as,

$$E_{\text{elas}} = \frac{A}{2}\sum_{\text{nn}}(x - R(\sigma_i, \sigma_j))^2 + \frac{B}{2}\sum_{\text{nnn}}(x\sqrt{2} - R_{\text{d}}(\sigma_i, \sigma_k))^2 \quad (5)$$

Figure 1 displays the elastic configurations of a rigid LS unit cell of square lattice for $\xi \neq 0$. According to eq 5, in the first configuration the nn springs are at rest, while the nnn springs (in red) are under tension. However, if the nnn distances are fixed to their equilibrium distance, $(2)^{1/2}(R^{\text{LL}} + \delta_R)$, the elastic energy will be stored in nn springs (figure in the right). The relaxed configuration, depicted in the center, corresponds to the mechanical equilibrium $\partial E_{\text{elas}}/\partial x = 0$ and shows the stressed character of all bonds (in red). In the general case, the analytic minimization (see Appendix II in the SI) of the elastic energy (eq 5) of rigid LS (i.e., all distances are equal to R^{LL}) and HL antiferro-like (i.e., all distances are R^{HL}) leads to the following nn relaxed distances,

$$R^{\text{LL}}_{\text{relax}} = R^{\text{LL}} + \frac{2\alpha}{1+2\alpha}\xi\delta_R \quad \text{and} \quad R^{\text{HL}}_{\text{relax}} = R^{\text{HL}} + \frac{\alpha}{1+2\alpha}\xi\delta_R \quad (6)$$

where $\alpha = (B/A)$ is the ratio between the nnn and nn elastic constants. One should note the linear dependence of the relaxed nn distances on ξ and their nonlinear dependence on α, which indicates the important role of the nnn elastic constant, which has not been considered in previous elastic models for SC solids. To keep the volume of LS lattice smaller than that of HS, one needs to fulfill the inequality, $R^{\text{LL}}_{\text{relax}} < R^{\text{HH}}$, which implies the following constraint, $\xi < \xi_{\text{max}} = (1+2\alpha)/2\alpha$, leading here to $\xi < 2.66$.

3. RESULTS AND DISCUSSION

We have carried out extensive Monte Carlo simulations (MC) based on a novel code written in CUDA[32] with the libraries of cuRand[33] and thrust,[34] and using the performance of Nvidia cores. We have "carefully" parallelized the MC algorithm for the spin state of the crystal in several clusters. In this study, the clusters have a size of 4×4 where we check the spin state of each molecule sequentially. In the simulations, where the simulated crystal size is $N_x \times N_y = 48 \times 24$, we have 12×6 clusters which means that the code checks 72 spin nodes each MC update.

Next, the lattice is relaxed in a deterministic way, using molecular dynamics method,[20] to reach the stable mechanical state. At each step, the code calculates the gradient of potential energy (eq 2) on each node in order to determine the force vector acting on every molecule $\vec{F} = -\vec{\nabla}\mathcal{H}_{\text{elas}}$. The obtained force field over the whole system is then normalized to the strongest modulus, and the lowest energy configuration is searched by relaxing the system in overdamped dynamics with a time step, $dt^2 = 0.002$. This procedure is repeated 3 times before checking the next 72 spin sites. The new positions of the molecules are then recalculated using the new force field with a strong damping to avoid oscillations.

The algorithm is repeated 16 times (number of molecules in one cluster), which defines one MC step (MCS). The thermal hysteresis loops are calculated by using 625 MCS as a waiting time to reach the stationary states at each temperature, and then the next 50 MCS are averaged to calculate the HS fraction, $n_{\text{HS}}(T)$.

We used here, as far as possible, realistic parameter values for the model. So we set, $R^{\text{HH}} = 9.4063$ Å and $R^{\text{LL}} = 9.167$ Å which led to lattice parameter expansion between the LS and the HS states $\delta_R = R^{\text{HH}} - R^{\text{LL}} = 0.24$ Å, in excellent agreement with experimental data.[35] The elastic constant values, $A = 8 \times 10^5$ K nm^{-2} and $B = 0.3A$, are chosen so as to have bulk modulus of some tens of GPa[22] as detailed in the Appendix III of the SI. The other parameter values are $\Delta = 281.5$ K and $\ln g = \ln(150) \simeq 5.01$, leading to a molar entropy change at the transition: $\Delta S = 41$ J K^{-1} mol^{-1} and a transition temperature $T_{\text{eq}} = 2\Delta/\left(k_{\text{B}} \ln g\right)$.

We have calculated the thermal-dependence of the HS fraction, $n_{\text{HS}} = (1 + \langle\sigma\rangle)/2$, as a function of T for different values of ξ. The results are summarized in Figure 2. The

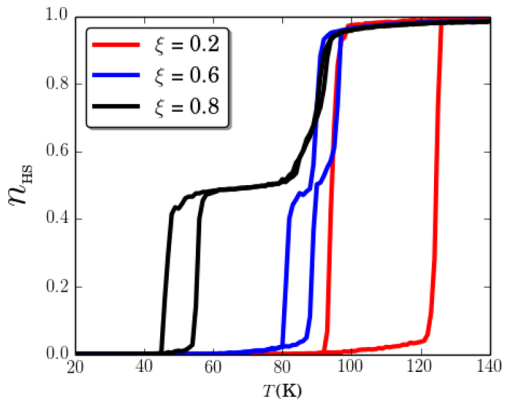

Figure 2. Thermal dependence of the HS fraction for different values of the elastic frustration ξ, showing usual first-order transition (red), two-step with two first-order phase transitions accompanied by hysteresis loops (blue), and two-step SC transition with a large plateau around $n_{\text{HS}} \sim 0.5$ (black). Notice the global shift of the transition temperatures to low-temperature regions as ξ increases. The parameters of the model were: $R^{\text{HH}} = 9.4063$ Å, $R^{\text{LL}} = 9.167$ Å ($R^{HL} = (R^{\text{HH}} + R^{\text{LL}})/2$) for the bond lengths, and $A = 8 \times 10^5$ Knm^{-2} (respectively, $B = 0.3A$) for nn (respectively, nnn) elastic constants, $\Delta = 281.5$ K and $\ln g \simeq 5$ for the ligand field and degeneracy ratio, respectively. The temperature sweep rate was 1 K every 675 MCS, which was the waiting time to reach the stationary state.

corresponding thermal evolution of the average nn bond lengths, ($\langle|\vec{r}_{ij}|\rangle$), given in Figure S1 of the SI, shows an increase of the LS bond lengths as ξ is increased. For relatively weak values of the frustration, for example $\xi = 0.2$, the behavior is that of the usual first-order transition (red curve) between the LS and the HS states accompanied by a thermal hysteresis loop. Increasing ξ value up to $\xi = 0.6$, the transition region is lowered, and the behavior changes to that of a two-step transition (blue curve) with two hysteresis loops separated by a small plateau. For higher values of ξ, such as $\xi = 0.8$ (black curve), the plateau widens and separates a 'hysteretic" first-order spin transition at low temperature ($T^{-}_{\text{eq}} \sim 50$ K) and a gradual one at higher temperature ($T^{+}_{\text{eq}} \sim 90$ K). The spatial

DOI: 10.1021/jacs.6b00049
J. Am. Chem. Soc. 2016, 138, 3202−3210

organizations of the HS fractions on heating and cooling, corresponding to the three thermal hysteresis of Figure 2, are given in the three movies S1−S3, available in the SI. In movie S1 (ξ = 0.2) the transformation on cooling (respectively, heating) from HS to LS (respectively, LS to HS) starts from the corners through the nucleation and propagation of a single domain of the stable LS (respectively, HS) phase inside the metastable HS (respectively, LS) phase. The situation is different for the two-step transitions (ξ = 0.6 and ξ = 0.8). For ξ = 0.6 (movie S2), on cooling, both spin transitions lead to a nucleation and growth process starting from the corners. On heating, the low-temperature spin transition shows also the emergence of ordered antiferro-elastic HS-LS-HS-LS (with antiphase boundaries) structures from the corners, whereas for the higher spin transition (around $T \sim 94$ K) between the AF and the HS states, we see the appearance of a significant amount of HS droplets in the "volume". This multidroplet nucleation process is caused by the strengthening of thermal fluctuations at this temperature combined with the weakening of the cooperativity by the increase of the elastic frustration. The domain growth mode is quite similar for the case ξ = 0.8, where we obtain a nucleation from the corners on heating and cooling for the hysteretic low-temperature spin transition, whereas the high-temperature transition (almost gradual) shows the presence of ramified structures and multidroplet nucleation, due to its weak cooperative character. One should notice, however, that the case of ξ = 0.8 is quite unusual, since on heating from the plateau region, the snapshots (movie S3) show the coexistence of several types of ordered patterns, such as, HS-LS-HS-LS, LS-HS-HS-HS-HS-LS (and its symmetric configuration) etc., attesting that spin-crossover solids with elastic frustration may behave as complex systems.

We would like to note here that the present results contrast with all previous theoretical investigations on the occurrence of multistep spin transitions in SC materials, which assumed the existence of ad-hoc antiferro-magnetic interactions, which unfortunately do not catch the essential physics of this problem. The elastic frustration is then at the heart of the multistability of SC solids.

To understand the conditions of occurrence of the various transitions observed in Figure 2, we performed a detailed energetic analysis. Let us consider the case of a simple hysteresis loop (red curve) of Figure 2. The transition temperatures between LS↔HS can be simply defined as $T_{\uparrow} = T(n_{HS} = 0.5)$ for heating (↑) and $T_{\downarrow} = T(n_{HS} = 0.5)$ for cooling (↓) processes. Similarly, for the two-step transitions (blue and black curves), the transition temperatures of the upper (+) and lower (−) hysteresis loops are roughly given by $T^{+}_{\downarrow\uparrow} = T(n_{HS} = 0.25)$ and $T^{-}_{\downarrow\uparrow} = T(n_{HS} = 0.75)$, respectively. The existence of a plateau at $n_{HS} = 0.5$ involves the condition, $|(\partial n_{HS}/\partial T)(T = T_{\downarrow\uparrow})| < |(\partial n_{HS}/\partial T)(T = T^{+}_{\downarrow\uparrow})|$.

Now, we investigate analytically the condition of occurrence of the two-step transition. For that, the Hamiltonian (eq1) was dissected (see Appendix IV in the SI) and rewritten under the form of an "Ising-like" model. There, we could identify the total effective field acting on a single spin site as equal to

$$h_i(x) = \Delta_{eff} - 2\delta_R(x - R^{HL})(A + 2B(1 - \xi)) + 2B{\delta_R}^2(1 - \xi)\xi \quad (7)$$

where $x = |\vec{r}_{ij}|$, in the approximation of a rigid lattice. Equation 7 shows that the effective "ligand field" acting on the molecule includes the usual ligand-field energy (Δ_{eff}) and an elastic field contribution arising from nn and nnn interactions. Considering that at the transition temperature the effective ligand field reverses its sign, it was possible to find the analytic dependence of the transition temperatures, T_{eq} and $T^{\pm}_{eq}$, corresponding respectively n_{HS} = 0.5 and n_{HS} = 0.25 and 0.75. These analytic expressions are given by

$$T_{eq}(\xi) = \frac{2\Delta}{k_B \ln g} - \frac{4B(\xi\delta_R)^2}{(1 + 2\alpha)k_B \ln g} \quad (8)$$

$$T^{\pm}_{eq}(\xi) = T_{eq}(\xi) \pm \frac{2B{\delta_R}^2}{k_B\, n\, g}\left(\xi^2 \frac{2\alpha}{1 + 2\alpha} - 2\xi + 1\right) \quad (9)$$

A remarkable elastic field energy contribution, $2\Delta_{elas} = -[4B(\xi\delta_R)^2/(1 + 2\alpha)]$ to the electronic ligand field, 2Δ, emerges in eq 8, shifting downward the transition temperatures, in agreement with the numerical results of Figure 2. This behavior is enhanced when the lattice parameter misfit δ_R or the nnn elastic interaction is increased. Consequently, we can consider that there is a one-step first-order transition when $T^{-}_{eq} > T_{eq} > T^{+}_{eq}$, which means that only the first equation in eq8 is valid. When the two-step transition behavior occurs, eq 9 becomes true, and in this case we satisfy the condition $T^{-}_{eq} < T_{eq} < T^{+}_{eq}$. This way, by increasing the frustration parameter ξ, the red thermal hysteresis of Figure 2 splits when $T_{eq}(\xi) = T^{\pm}_{eq}(\xi)$, which defines a bifurcation point taking place at

$$\xi_{th} = \frac{1 + 2\alpha \pm \sqrt{1 + 2\alpha}}{2\alpha} \quad (10)$$

It is interesting to notice that the threshold value, ξ_{th}, above which the double step transition takes place, depends only on the ratio between the nnn and nn elastic constants. Within the value $\alpha = B/A = 0.3$ used in this work, two values ξ_{th} = 0.55848 and 4.77485 (excluded) are obtained. This prediction matches very well the value $\xi_{th} \approx 0.57$ found by MC simulations, depicted in the phase diagram of Figure 3, in

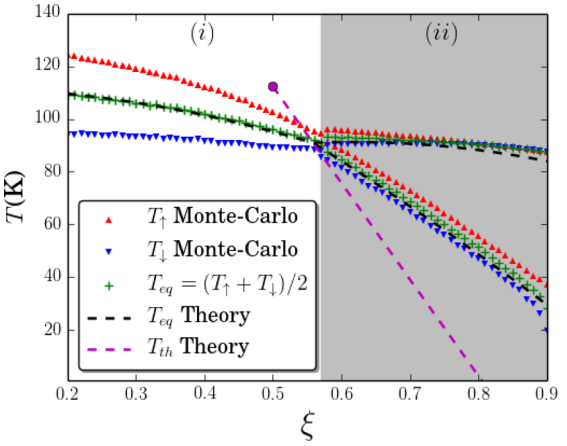

Figure 3. Calculated diagram illustrating the ξ-dependence of the transition temperatures. Red and blue triangles are MC results of $T_{\uparrow}$ and $T_{\downarrow}$. Crosses represent MC transition temperatures ($=(T_{\uparrow} + T_{\downarrow})/2$) and the dashed black line is the analytical prediction of eqs 8and 9. Region (i) and region (ii), separated by the line $\xi = \xi_{th} \sim 0.558$, delimit the regions of one-step and two-step spin transition, respectively. The oblique dashed line stands for the geometrical locus of the threshold points (ξ_{thresh}, T_{thresh}) as a function of α. See text for more explanation. The parameter values are the same as those of Figure 2, except for ξ, which was varied in the interval [0.2:0.9].

DOI: 10.1021/jacs.6b00049
J. Am. Chem. Soc. 2016, 138, 3202−3210

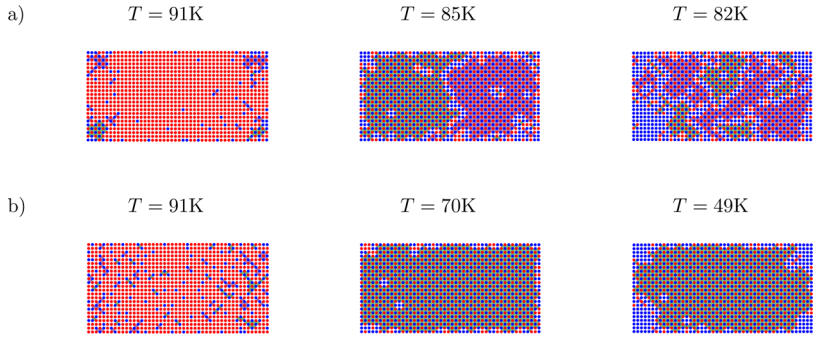

Figure 4. Snapshots of the lattice configurations along the thermal transition on cooling. Top (respectively, bottom) panels correspond to the blue (respectively, black) curve of Figure 2 for which $\xi = 0.6$ (respectively, $\xi = 0.8$). From left to right for both cases, the middle panels correspond to the plateau region. Antiphase boundaries (represented in gray) emerge for $\xi = 0.6$ at 85 and 82 K, while we see a "perfect" AF order for $\xi = 0.8$ at 70 and 49 K. Red (respectively, blue) points correspond to HS (respectively, LS) molecules. See text for more explanation.

which we present the ξ-dependence of the transition temperatures. There, the dashed black line corresponds to the analytical expressions of the equilibrium transition temperatures $T_{eq}(\xi)$, given by eqs 8 and 9, while the crosses are those derived from MC simulations as $T_{eq} = \left(T_{\downarrow} + T_{\uparrow}\right)/2$. The blue (respectively, red) triangles correspond to lower $T_{\downarrow}$ (respectively, upper, $T_{\uparrow}$) transition temperatures of the MC thermal hysteresis, which, of course, depend on the temperature sweeping rate, since they correspond to the end of metastability. So, according to ξ values, three regions can be identified in the phase diagram: (i) a one-step first-order transition for $0 < \xi < 0.57$; (ii) two-step transition for $0.57 < \xi < 1$; and (iii) an incomplete (or partial) SC transition for $\xi > \xi_{inc}$. In the region of two-step transitions, the thermal width of the plateau is given $\Delta T = (4B{\delta_R}^2/k_B \ln g)[(2\alpha 1 + 2\alpha)\xi 2 - 2\xi + 1]$. This double step transition exists as soon as $T_{\downarrow}^{-} > 0$ K. To complete the phase diagram of Figure 3, we have calculated the geometrical locus of bifurcation points (given by eq 10) as a function of α in T-ξ diagrams. The obtained curve (see SI for the details of the calculations) is plotted in bold dashed line.

The value of the threshold transition temperature, $T_{th}(\xi_{th})$ at $\xi = \xi_{th}$, separating the one- and two-step transition areas, is calculated by introducing eq 10 into the eq 8, which gives

$$T_{th}(\xi_{th}) = \frac{2\Delta}{k_B \ln g} - \frac{2A{\delta_R}^2}{k_B \ln g}(2\xi_{th} - 1) \tag{11}$$

where ξ_{th} is α-dependent (eq 10). Increasing the elastic ratio α results in a decrease of $T_{th}(\xi_{th})$. Consequently, we found that there is a maximum ratio α_{max} allowing the existence of a two-step transition; at this value $T_{th} = 0$ K, which leads to

$$\alpha_{max} = \frac{\frac{2\Delta}{A{\delta_R}^2}}{\left(1 - \frac{2\Delta}{A{\delta_R}^2}\right)^2} \tag{12}$$

As long as we do not have an analytical expression for $T_{\downarrow}^{-}$, we can safely approximate the threshold value ξ_{inc} at which the incomplete spin transition emerges as given by the relation $T_{eq}^{-} = 0$. The expression of ξ_{inc} is then obtained as

$$\xi_{inc} = -\frac{\sqrt{1 + 2\alpha}}{2(1 - \alpha)}\left[\sqrt{1 + 2\alpha} \pm \sqrt{3 + 2(1 - \alpha)\frac{\Delta}{B{\delta_R}^2}}\right] \tag{13}$$

Within the parameter values used in the simulation we evaluated $\xi_{inc} = 1.045$ (the negative value is ignored). Nevertheless, in the simulations an incomplete transition could appear at $\xi < 1.045$, for two reasons. First, the condition $T_{eq}^{-} = 0$ overestimates the value of ξ_{inc}, and second, even for $T_{\downarrow}^{-} > 0$ the obtained phase in the plateau region may stay "frozen" due to kinetic effect (due to the lack of sufficient thermal fluctuations).

One of the most important features of the two-step transition in SC solids is the self-organization of the HS and LS domains in the plateau region. Thus, in the case of $Fe(2\text{-pic})_3Cl_2EtOH$ (2-pic = 2-amino-methyl-pyridine),[36,37] for example, which shows a two-step spin transition with a plateau, Burgi et al.[38] demonstrated using X-ray diffraction experiments that in the plateau region, which corresponds to $n_{HS} \simeq 0.5$, this system self-organizes as a succession of globally LS and HS layers, which was one of the first demonstrations of the emergence of complexity in spin-crossover solids. More recently, X-ray diffraction investigations[39−43] have evidenced several types of organization, like usual antiferro-magnetic-like (HS-LS-HS-LS···) configurations, but also more subtle ones like (HS-HS-LS-LS-HS-HS-LS···), and even much more complex 2D patterns and modulated HS concentration structures with a vector of modulation which can be commensurate or incommensurate with the lattice parameter. So, in this context, we investigate the type of spatial organization of the spin states inside the plateau upon the two-step transitions of Figure 2. Selected snapshots of the spatial organization of the system are shown in Figure 4 for the frustration values, $\xi = 0.6$ and $\xi = 0.8$, corresponding to the blue and black curves of Figure 2, respectively. For $\xi = 0.6$ (respectively, $\xi = 0.8$), the snapshots are given at temperatures 91, 85, and 82 K (respectively, 91, 70, and 49 K), and the corresponding HS fractions are $n_{HS} \simeq 0.93$, $n_{HS} \simeq 0.5$, and $n_{HS} \simeq 0.4$ (respectively, $n_{HS} \simeq 0.9$, $n_{HS} \simeq 0.5$, and $n_{HS} \simeq 0.45$).

We see clearly, for both cases, that the system converts from an ordered HS state to an intermediate ordered antiferro-like structure, in which each HS (respectively, LS) site is surrounded by LS (respectively, HS) sites. In addition, we found in the case $\xi = 0.6$, the presence of antiphase boundaries (see Figure 4), which appeared disordered due to thermal fluctuations. Here, we recall that originally, antiphase boundaries (APB) have been extensively studied in metal alloys and in semiconductors.[44,45] They constitute interfaces separating two macroscopic phases having the same order parameter value, and so they can be considered as topological

DOI: 10.1021/jacs.6b00049
J. Am. Chem. Soc. 2016, 138, 3202−3210

defects. In the present case, the APB separate two antiferro-magnetic-like structures having an order parameter value n_{HS} = 1/2. To help the reader well identify the two types of antiferro structures, which represent two degenerate states, we highlighted them with different colors for each "phase". Since the energy of these two states is equal, the APB can move freely without any energy supply. The case of ξ = 0.8 is also interesting since it shows an almost "perfect" antiferro-elastic ordering in the plateau region [50:85] K. For this case, it was possible to define two sublattices, A and B, for which we followed the thermal dependencies of their associated HS fractions, n^A_{HS} and n^B_{HS}, which are sketched in Figure S2 of the SI. Both $n^A_{HS}(T)$ and $n^B_{HS}(T)$ show bifurcation points denoting the existence of symmetry breaking between the two sublattices. This is also confirmed by the thermal evolution of the order parameter, $n^A_{HS} - n^B_{HS}$, given in Figure 5, where we

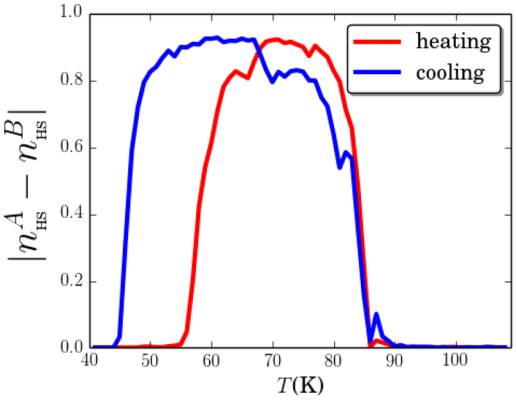

Figure 5. Thermal dependence of the difference of HS fractions, $\|n^A_{HS} - n^B_{HS}\|$, of the two sublattices A and B in the coexistence region of the plateau for ξ = 0.8, corresponding to the black curve of Figure 2. Second-order phase transitions in each sublattice are revealed, announcing the presence of a symmetry breaking between A and B sublattices. The red (respectively, blue) curve corresponds to the heating (respectively, cooling) process. The results have been averaged over 6 different random seeds.

observed evidence of symmetry breaking at T = 55 and 88 K (respectively, 45 and 88 K) on heating (respectively, cooling), denoting the existence of second-order phase transitions. The fact that the order parameter, $n^A_{HS}-n^B_{HS}$, does not reach 1 in the middle of the plateau region is due to the presence of disorder at the corners and edges of the lattice (see Figure 4).

Increasing ξ values above ξ = 1.045 causes the shift of the down thermal hysteresis of Figure 2 to low-temperature regions (see eq 8), until reaching the limit, T^-_{eq} = 0, above which the intermediate phase (the plateau) is stabilized until 0 K, as depicted in Figure 6. However, the incomplete (or partial) spin transition may happen for frustration values, $\xi \lesssim 1.045$, due to kinetic effects related to the velocity of the temperature sweep rate of the Monte Carlo procedure. The system is then trapped in the plateau region (as for ξ = 1 in Figure 6) due to the lack of thermal fluctuations and subsequent increase of the lifetime of the metastable states as shown in Figure 6. Interestingly, we have also observed at T = 10 K for the value ξ = 1, an almost perfectly ordered AF domain, as shown in Figure 7, where we give the spatial organization of the HS (red dots) and LS (blue dots) sites. Besides the electronic configuration of the system, the study of the elastic organization can be investigated through

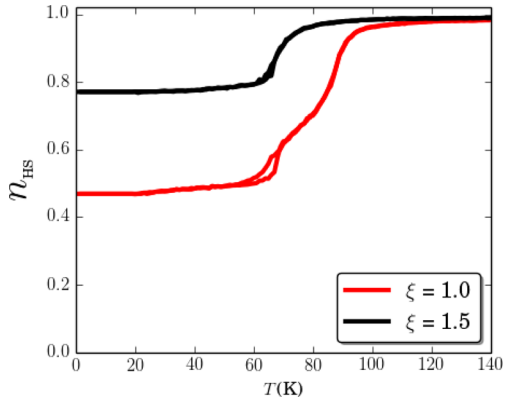

Figure 6. Thermal dependence of the HS fraction in the case of strong frustration values, ξ = 1.0 and ξ = 1.5, showing the occurrence on incomplete spin transition. The other parameter values are the same as those of Figure 2.

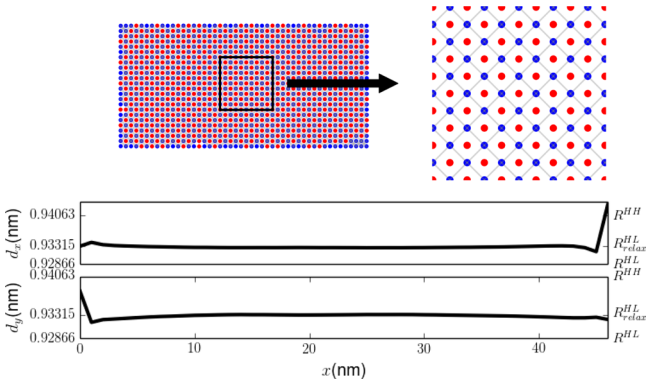

Figure 7. Top: snapshots showing the perfect antiferro-like spatial organization of the HS/LS sites corresponding to Figure 6 at T = 10 K for ξ = 1.0. The molecules' positions are represented by circles of different colors: HS (red) and LS (blue). Top right: an enlarged view of the squared region. Gray dashed lines linking the LS molecules are added for clarity. Bottom: longitudinal (d_x) and transverse (d_y) lattice parameter distances (see eq 14) along x-direction at $j = N_y/2$, showing a uniform behavior except around the lattice edges. The obtained values match very well the analytical predicted value R^{HL}_{relax} given in eq 6.

the spatial dependence of the longitudinal d_x and the transverse d_y nn bond lengths along the x-axis. Their expressions are

$$d_x(x) = |\vec{r}_{i+1,j} - \vec{r}_{i,j}| \quad \text{and} \quad d_y(x) = |\vec{r}_{i,j+1} - \vec{r}_{i,j}| \qquad (14)$$

We see in the bottom figures of Figure 7 that, except at the border of the lattice, both distances, d_x and d_y, are invariant by translation, and their values perfectly match the analytical prediction of R^{HL}_{relax} given in eq 6, confirming the antiferro-elastic ordered character of this phase. On the other hand, it is worth noticing that for frustration parameter values ξ < 1.0, leading to a two-step transition, we could find a value of Δ and g for which $T^-_{\downarrow} \sim 0$ K, which then consequently leads to an incomplete spin transition, which are often observed experimentally[5,40,46] by changing the size of the ligand or the anion.[47−58]

If we increase further the frustration ratio, ξ, the HS residual fraction appearing at low temperature increases (black curve in Figure 8) and reaches the value $n_{HS} \simeq 0.77$ for ξ = 1.5. For this strong frustration, a new type of organization in the plateau region is found. Figure 1 presents the corresponding spatial electro-elastic configuration emerging at T = 10 K. This type of

DOI: 10.1021/jacs.6b00049
J. Am. Chem. Soc. 2016, 138, 3202−3210

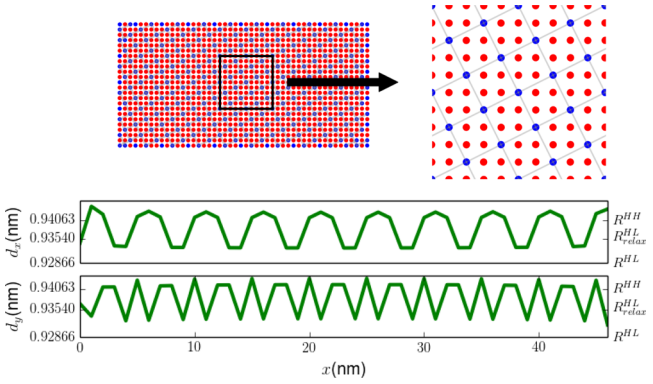

Figure 8. Top: snapshots showing the occurrence of a complex spatial organization of the HS/LS sites for $n_{HS} \sim 3/4$ corresponding to the incomplete spin transition of Figure 6 for $\xi = 1.5$ at $T = 10$ K. Red (respectively, blue) dots represent HS (LS) sites. Gray dashed lines linking the LS molecules are added for clarity. Bottom: longitudinal (d_x) and transverse (d_y) lattice parameter distances (see eq 14) along x-direction (at $j = N_y/2$) showing a modulated structure. The modulation is anisotropic but commensurate along the x and y directions with the lattice parameter. See text for more explanation.

structure is difficult to predict analytically from the simple analysis of the relaxed energy of the different configurations of the square unit cell of Figure 1, because the obtained self-organized pattern involves the interplay between several unit cells. We have investigated the elastic properties of the ordered state of Figure 8 by inspecting the behavior of the longitudinal $d_x(x)$ and the transverse $d_y(x)$ interatomic distances along the x-direction. The results, depicted in the bottom of Figure 8, clearly indicate the presence of periodic spatial elastic modulations for both nn distances. In particular $d_x(x)$ (as well as $d_y(y)$, not shown) exhibits a modulation which is commensurate with the lattice parameter. In particular we notice here that $d_x(x)$ exceeds locally at its maximum values, those (R^{HH}) of the relaxed HS state, indicating that the whole lattice remains under tension in the plateau region. We checked that the model in its current state may allow obtaining incommensurate modulations for some values of the frustration parameter at low temperature, similarly to those observed in Frenkel-Kontorova model[59] for epitaxial growth. This specific part, which needs particular attention, will be developed elsewhere.

It is worth mentioning that the results of Figure 8 recall the recent experimental findings of X-ray investigations,[39,40] showing the occurrence of HS/LS modulated structures in two-step spin-crossover compounds. In particular HS-HS-LS-LS··· configurations were reported in the experimental literature. We could obtain these structures using the current model, but then we had to consider an anisotropic deformation of the unit cell upon the SC transition. This is also another extension of the model, which will be considered elsewhere.

Remarkably, if we inspect in details the shape of the red curve of Figure 6 (obtained for $\xi = 1$), we see the presence of a second plateau around $T \simeq 80$ K for $n_{HS} \simeq 0.7$, announcing the presence of a second structural phase, which is stabilized in the plateau of the black curve for $\xi = 1.5$. This new pattern shows a complex organized structure where the LS sites appear every four HS sites. This type of organization causes the modulation of the nn distances between the sites, as shown by the spatial dependence of d_x and d_y along the x direction. Much more complex organizations, leading to HS-HS-LS-HS-HS-LS-HS-HS-LS structures, can also be found according to the values of ξ. Much more interesting, patterns mixing different types of organizations may also emerge in the simulations, especially on heating in the case of double-step transitions, as the reader can see in movies S1−S3 given in the SI. Furthermore, if we start at low temperature ($T = 40$ K, for example) with $\xi = 1$ and we increase the value of the frustration parameter ξ up to 1.5, we observe a change of spatial self-organization of Figure 7, which first becomes disordered before the emergence of long-range patterns corresponding to those of Figure 8. Selected snapshots corresponding to this crossover behavior are displayed in Figure 9. It is clear that the role of temperature would deserve another study.

4. CONCLUSION

In conclusion, we reported on the first full elastic model enabling the description of the two-step spin transition in SC solids, caused by the existence of elastic frustration in the lattice. In real systems, this frustration may be caused by the presence of covalent (respectively, weak) bonds enhancing the lattice rigidity (respectively, softness) in some directions, which may hinder (respectively, favor) the deformation in some particular directions. This type of anisotropy is present in many SC materials. In the current work, we studied the specific case of a rigid 2D lattice, in which a controlled frustration (through a parameter ξ) takes place along the diagonals. To be realistic, the model is written so as to keep the HS state free from any frustration. Our study reproduces several experimentally observed situations, among them the one-step first-order transition, two-step transitions, and partial SC transitions, also called incomplete spin transitions. In addition, we observed that according to the degree of frustration, a spatial order of the HS-LS species emerges in the plateau region. The type of order and its complexity depend on ξ values. For relatively small ξ values an AF-like order was evidenced in excellent agreement with experimental observations, while for strong frustration more complex organizations were found, among which a spatial modulation of the bond-length distances was revealed, here also in excellent agreement with very recent X-ray diffraction investigations. We would like to mention here, to the best of our knowledge, that existing spin-based models which studied the problem of the two-step SC transition included explicitly antiferro-magnetic-like interactions in the Hamiltonian. On the

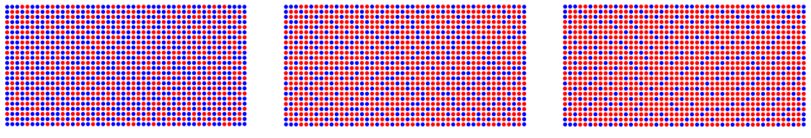

Figure 9. Snapshots showing the crossover between two types of spatial organization of the HS and LS sites, obtained by varying the frustration rate ξ at $T = 40$ K. From left to right, $\xi = 1.2$, 1.39, and 1.79. The configurations corresponding to $\xi = 1$ for which $n_{HS} = 0.5$ and $\xi = 1.8$ are given in Figures 7 and 8.

DOI: 10.1021/jacs.6b00049
J. Am. Chem. Soc. 2016, 138, 3202−3210

contrary, here the two-step transition emerges as a result of competing elastic interactions resulting from the presence of elastic frustration along certain crystallographic directions. As a result, it is extremely difficult to predict in advance the self-organized structures which will be stabilized in the plateau region. Anisotropic next-nearest-neighbor Ising-like models[60,61] combined with elastic interactions may represent an appropriate option to describe the self-organized structures arising from a frustrated SC solid, using a phenomenological interaction between spin states.

Coming back to our elastic description, we would like to stress the prediction of the existence of free APB in the antiferro-elastic region and its different nature compared to the usual HS/LS interface observed by optical microscopy[35,62,63] during the first-order transition of a SC single crystal. The latter separates two phases with different order parameter values, namely $n_{HS} = 0$ and $n_{HS} = 1$, whereas APB separates two regions with the same order parameter (here $n_{HS} = 1/2$). Since both of them emerge from the long-range nature of the elastic interactions, they allow macroscopic domain growth from the corners in the model. The dynamics of these APB and their observations constitute a future experimental challenge.

Finally, it is important to note here that the current model offers several extensions related to the choice of the directions of the elastic frustration, which may lead to multistable spin transitions. The complex interplay between the electronic and the elastic structures under light irradiation and the subsequent system relaxation also opens the opportunity of observing nonlinear dynamics, pattern formation of complex elastic structures, as well as hidden states or hidden hysteresis, which can be revealed by the competition with light irradiation, which favors disorder, and elastic long-range elastic interactions, which build up long-range order. Furthermore, the quantitative comparison to a real system requires identification of the source of the elastic frustration in the structural data and adaptation of the model to the possible anisotropy of the unit cell deformation upon spin transition. This work is in progress.

■ ASSOCIATED CONTENT

Supporting Information

The Supporting Information is available free of charge on the ACS Publications website at DOI: 10.1021/jacs.6b00049.

Section I: Movies S1−S3 describing the thermal transitions for different elastic frustration values. Section II: detailed calculations of the spin state dependence of the nn and nnn distances, including frustration effects. Section III: Detailed calculations of the analytic expressions of the relaxed nn equilibrium distance. Section IV: mathematical developments related to the frustration dependence of the transition temperature for one-step and two-step transitions. Section V: Additional results of the thermal dependence of the lattice parameter and HS fraction as a function of the frustration rate. Section VI: expressions of the threshold value of the frustration parameter separating the regions of one-step and two-steps spin transitions. Section VII: Details about the numerical procedure for the CUDA parallelized algorithm (PDF)

Movie S1, video showing the thermal transitions for $\xi = 0.2$ (AVI)

Movie S2, video showing the thermal transitions for $\xi = 0.6$ (AVI)

Movie S3, video showing the thermal transitions for $\xi = 0.8$ (AVI)

■ AUTHOR INFORMATION

Corresponding Author

*kbo@physique.uvsq.fr

Notes

The authors declare no competing financial interest.

■ ACKNOWLEDGMENTS

The authors acknowledge S. Pillet, E. Collet, and S. Triki for fruitful discussions. This work was supported by the Université Paris-Saclay, Université de Versailles, CNRS, and the "Agence Nationale de la Recherche" (ANR project BISTA-MAT: ANR-12-BS07-0030-01), which are deeply acknowledged.

■ REFERENCES

(1) Gütlich, P.; Hauser, A. *Coord. Chem. Rev.* **1990**, *97*, 1−22.

(2) Gütlich, P.; Gaspar, A. B.; Garcia, Y. *Beilstein J. Org. Chem.* **2013**, *9*, 342−391.

(3) Bonnet, S.; Siegler, M. A.; Costa, J. S.; Molnár, G.; Bousseksou, A.; Spek, A. L.; Gamez, P.; Reedijk, J. *Chem. Commun.* **2008**, 5619−5621.

(4) Bonnet, S.; Molnár, G.; Sanchez Costa, J.; Siegler, M. A.; Spek, A. L.; Bousseksou, A.; Fu, W.-T.; Gamez, P.; Reedijk, J. *Chem. Mater.* **2009**, *21*, 1123−1136.

(5) Molnár, G.; Guillon, T.; Moussa, N. O.; Rechignat, L.; Kitazawa, T.; Nardone, M.; Bousseksou, A. *Chem. Phys. Lett.* **2006**, *423*, 152−156.

(6) Sciortino, N. F.; Scherl-Gruenwald, K. R.; Chastanet, G.; Halder, G. J.; Chapman, K. W.; Létard, J.-F.; Kepert, C. J. *Angew. Chem.* **2012**, *124*, 10301−10305.

(7) Gütlich, P.Metal Complexes. In *Structure and Bonding*; Springer: Berlin Heidelberg, 1981; Vol. *44*; pp 83−195.

(8) Hauser, A. *Coord. Chem. Rev.* **1991**, *111*, 275−290.

(9) Kahn, O.; Kröber, J.; Jay, C. *Adv. Mater.* **1992**, *4*, 718−728.

(10) Gütlich, P.; Goodwin, H. A. Spin Crossover in Transition Metal Compounds I-III. In *Topics in Current Chemistry*; Springer-Verlag Berlin Heidelberg: Berlin, Heidelberg, NY, 2004; Vol. *233, 234, 235*.

(11) Freysz, E.; Montant, S.; Létard, S.; Létard, J. F. *Chem. Phys. Lett.* **2004**, *394*, 318−323.

(12) Fouché, O.; Degert, J.; Jonusauskas, G.; Daro, N.; Létard, J. F.; Freysz, E. *Phys. Chem. Chem. Phys.* **2010**, *12*, 3044−52.

(13) Halcrow, M. A. *Spin-Crossover Materials: Properties and Applications*; John Wiley and Sons Ltd: West Sussex, UK, 2013.

(14) Jureschi, C. M.; Linares, J.; Rotaru, A.; Ritti, M. H.; Parlier, M.; Dîrtu, M. M.; Wolff, M.; Garcia, Y. *Sensors* **2015**, *15*, 2388.

(15) Spiering, H.; Willenbacher, N. *J. Phys.: Condens. Matter* **1989**, *1*, 10089.

(16) Nishino, M.; Boukheddaden, K.; Konishi, Y.; Miyashita, S. *Phys. Rev. Lett.* **2007**, *98*, 247203.

(17) Nishino, M.; Enachescu, C.; Miyashita, S.; Boukheddaden, K.; Varret, F. m. c. *Phys. Rev. B: Condens. Matter Mater. Phys.* **2010**, *82*, 020409.

(18) Nicolazzi, W.; Pillet, S.; Lecomte, C. *Phys. Rev. B: Condens. Matter Mater. Phys.* **2008**, *78*, 174401.

(19) Enachescu, C.; Nishino, M.; Miyashita, S.; Hauser, A.; Stancu, A.; Stoleriu, L. *EPL (Europhysics Letters)* **2010**, *91*, 27003.

(20) Enachescu, C.; Stoleriu, L.; Stancu, A.; Hauser, A. *Phys. Rev. Lett.* **2009**, *102*, 257204.

(21) Nishino, M.; Enachescu, C.; Miyashita, S.; Rikvold, P. A.; Boukheddaden, K.; Varret, F. *Sci. Rep.* **2011**, *1*.srep0016210.1038/srep00162

(22) Slimani, A.; Boukheddaden, K.; Varret, F.; Oubouchou, H.; Nishino, M.; Miyashita, S. *Phys. Rev. B: Condens. Matter Mater. Phys.* **2013**, *87*, 014111.

(23) Klinduhov, N.; Boukheddaden, K. *J. Phys. Chem. Lett.* **2016**, *7*, 722−727.
(24) Bousseksou, A.; Nasser, J.; Linares, J.; Boukheddaden, K.; Varret, F. *J. Phys. I* **1992**, *2*, 1381−1403.
(25) Bousseksou, A.; Varret, F.; Nasser, J. *J. Phys. I* **1993**, *3*, 1463−1473.
(26) Boukheddaden, K.; Linares, J.; Codjovi, E.; Varret, F.; Niel, V.; Real, J. A. *J. Appl. Phys.* **2003**, *93*, 7103−7105.
(27) Nishino, M.; Boukheddaden, K.; Miyashita, S.; Varret, F. *Phys. Rev. B: Condens. Matter Mater. Phys.* **2003**, *68*, 224402.
(28) Nasser, J.; Boukheddaden, K.; Linares, J. *Eur. Phys. J. B* **2004**, *39*, 219−227.
(29) Nishino, M.; Miyashita, S. *Phys. Rev. B: Condens. Matter Mater. Phys.* **2013**, *88*, 014108.
(30) Setifi, F.; Charles, C.; Houille, S.; Thétiot, F.; Triki, S.; Gómez-García, C. J.; Pillet, S. *Polyhedron* **2013**, *61*, 242−247.
(31) Boukheddaden, K.; Shteto, I.; Hôo, B.; Varret, F. *Phys. Rev. B: Condens. Matter Mater. Phys.* **2000**, *62*, 14796−14805.
(32) *CUDA*,Compute unified device architecture C programming guide; Nvidia Corp., 2007.
(33) Nandapalan, N.; Brent, R. P.; Murray, L. M.; Rendell, A. P. High-Performance Pseudo-Random Number Generation on Graphics Processing Units. In *Parallel Processing and Applied Mathematics: 9th International Conference, PPAM 2011, Torun, Poland, September 11−14, 2011. Revised Selected Papers, Part I*; Wyrzykowski, R., Dongarra, J., Karczewski, K., Waśniewski, J., Eds.; Springer Berlin Heidelberg: Berlin, Heidelberg, 2012; pp 609−618.
(34) Hoberock, J.; Bell, N.*Thrust*: A Parallel Template Library,2010.
(35) Sy, M.; Varret, F.; Boukheddaden, K.; Bouchez, G.; Marrot, J.; Kawata, S.; Kaizaki, S. *Angew. Chem.* **2014**, *126*, 7669−7672.
(36) Hauser, A. *Comments Inorg. Chem.* **1995**, *17*, 17.
(37) Ogawa, Y.; Ishikawa, T.; Koshihara, S.; Boukheddaden, K.; Varret, F. *Phys. Rev. B: Condens. Matter Mater. Phys.* **2002**, *66*, 073104.
(38) Chernyshov, D.; Hostettler, M.; Törnroos, K. W.; Bürgi, H.-B. *Angew. Chem., Int. Ed.* **2003**, *42*, 3825−3830.
(39) Pillet, S.; Bendeif, E.-E.; Bonnet, S.; Shepherd, H. J.; Guionneau, P. *Phys. Rev. B: Condens. Matter Mater. Phys.* **2012**, *86*, 064106.
(40) Collet, E.; Watanabe, H.; Bréfuel, N.; Palatinus, L.; Roudaut, L.; Toupet, L.; Tanaka, K.; Tuchagues, J.-P.; Fertey, P.; Ravy, S.; Toudic, B.; Cailleau, H. *Phys. Rev. Lett.* **2012**, *109*, 257206.
(41) Gaspar, A. B.; Ksenofontov, V.; Reiman, S.; Gutlich, P.; Thompson, A. L.; Goeta, A. E.; Munoz, M. C.; Real, J. A. *Chem. - Eur. J.* **2006**, *12*, 9289−98.
(42) Murnaghan, K. D.; Carbonera, C.; Toupet, L.; Griffin, M.; Dîrtu, M. M.; Desplanches, C.; Garcia, Y.; Collet, E.; Létard, J.-F.; Morgan, G. G. *Chem. - Eur. J.* **2014**, *20*, 5613−5618.
(43) Fitzpatrick, A. J.; Trzop, E.; Muller-Bunz, H.; Dirtu, M. M.; Garcia, Y.; Collet, E.; Morgan, G. G. *Chem. Commun.* **2015**, *51*, 17540−17543.
(44) Vanderbilt, D.; Lee, C. *Phys. Rev. B: Condens. Matter Mater. Phys.* **1992**, *45*, 11192−11201.
(45) Holt, D. *J. Phys. Chem. Solids* **1969**, *30*, 1297−1308.
(46) Halcrow, M. A. *Coord. Chem. Rev.* **2009**, *253*, 2493−2514.
(47) Claude, R.; Real, J. A.; Zarembowitch, J.; Kahn, O.; Ouahab, L.; Grandjean, D.; Boukheddaden, K.; Varret, F.; Dworkin, A. *Inorg. Chem.* **1990**, *29*, 4442−4448.
(48) Dîrtu, M. M.; Schmit, F.; Naik, A. D.; Rotaru, A.; Marchand-Brynaert, J.; Garcia, Y. *Hyperfine Interact.* **2012**, *205*, 69−73.
(49) Dîrtu, M. M.; Gillard, D.; Naik, A. D.; Rotaru, A.; Garcia, Y. Weak cooperativity in selected iron(II) 1D coordination polymers. In *ICAME 2011: Proceedings of the 31st International Conference on the Applications of the Mössbauer Effect (ICAME 2011) held in Tokyo, Japan, 25−30 September 2011*; Yoshida, Y., Ed.; Springer Netherlands: Dordrecht, 2013; pp 223−227.
(50) Fujigaya, T.; Jiang, D.-L.; Aida, T. *J. Am. Chem. Soc.* **2005**, *127*, 5484−5489.
(51) Dîrtu, M. M.; Rotaru, A.; Gillard, D.; Linares, J.; Codjovi, E.; Tinant, B.; Garcia, Y. *Inorg. Chem.* **2009**, *48*, 7838−7852.
(52) Garcia, Y.; Campbell, S. J.; Lord, J. S.; Linares, J.; Dîrtu, M. M.; Vendrell Pérez, A.; Boland, Y.; Ksenofontov, V.; Gütlich, P. *Hyperfine Interact.* **2014**, *226*, 217−221.
(53) Bushuev, M. B.; Lavrenova, L. G.; Shvedenkov, Y. G.; Varnek, V. A.; Sheludyakova, L. A.; Volkov, V. V.; Larionov, S. V. *Russ. J. Coord. Chem.* **2008**, *34*, 190−194.
(54) Verat, A. Y.; Ould-Moussa, N.; Jeanneau, E.; Le Guennic, B.; Bousseksou, A.; Borshch, S. A.; Matouzenko, G. S. *Chem. - Eur. J.* **2009**, *15*, 10070−10082.
(55) Pfaffeneder, T.; Bauer, W.; Weber, B. *Z. Anorg. Allg. Chem.* **2010**, *636*, 183−187.
(56) Martínez, V.; Gaspar, A.; Muñoz, M.; Bukin, G.; Levchenko, G.; Real, J. *Chem. - Eur. J.* **2009**, *15*, 10960−10971.
(57) Hamon, P.; Thépot, J.-Y.; Le Floch, M.; Boulon, M.-E.; Cador, O.; Golhen, S.; Ouahab, L.; Fadel, L.; Saillard, J.-Y.; Hamon, J.-R. *Angew. Chem., Int. Ed.* **2008**, *47*, 8687−8691.
(58) Wöhlert, S.; Tomkowicz, Z.; Rams, M.; Ebbinghaus, S. G.; Fink, L.; Schmidt, M. U.; Näther, C. *Inorg. Chem.* **2014**, *53*, 8298−8310.
(59) de Lange, C.; Janssen, T. *J. Phys. C: Solid State Phys.* **1981**, *14*, 5269.
(60) Selke, W. *Phys. Rep.* **1988**, *170*, 213−264.
(61) Boukheddaden, K.; Linares, J.; Tanasa, R.; Chong, C. *J. Phys.: Condens. Matter* **2007**, *19*, 106201.
(62) Slimani, A.; Varret, F.; Boukheddaden, K.; Garrot, D.; Oubouchou, H.; Kaizaki, S. *Phys. Rev. Lett.* **2013**, *110*, 087208.
(63) Sy, M.; Garrot, D.; Slimani, A.; Páez-Espejo, M.; Varret, F.; Boukheddaden, K. *Angew. Chem.* **2016**, *128*, 1787.

DOI: 10.1021/jacs.6b00049
J. Am. Chem. Soc. 2016, 138, 3202−3210